Ba_2NiOsO_6: A Dirac-Mott insulator with ferromagnetism near 100 K

Hai L. Feng,[1,2,*] Stuart Calder,[3] Madhav Prasad Ghimire,[4,5,†] Ya-Hua Yuan,[1,6] Yuichi Shirako,[7,‡] Yoshihiro Tsujimoto,[1] Yoshitaka Matsushita,[8] Zhiwei Hu,[2] Chang-Yang Kuo,[2] Liu Hao Tjeng,[2] Tun-Wen Pi,[9] Yun-Liang Soo,[9,10] Jianfeng He,[1,6] Masahiko Tanaka,[11] Yoshio Katsuya,[11] Manuel Richter,[4,12] and Kazunari Yamaura[1,6]

[1]*Research Center for Functional Materials, National Institute for Materials Science, 1-1 Namiki, Tsukuba, Ibaraki 305-0044, Japan*

[2]*Max Planck Institute for Chemical Physics of Solids, Nöthnitzer Strasse 40, 01187 Dresden, Germany*

[3]*Quantum Condensed Matter Division, Oak Ridge National Laboratory, Oak Ridge, Tennessee 37831, USA*

[4]*Leibniz Institute for Solid State and Materials Research, IFW Dresden, P.O. Box 270116, D-01171 Dresden, Germany*

[5]*Condensed Matter Physics Research Center, Butwal-13, Rupandehi, Lumbini, Nepal*

[6]*Graduate School of Chemical Sciences and Engineering, Hokkaido University, North 10 West 8, Kita-ku, Sapporo, Hokkaido 060-0810, Japan*

[7]*Department of Chemistry, Gakushuin University, 1-5-1 Mejiro, Toshima-ku, Tokyo 171-8588, Japan*

[8]*Materials Analysis Station, National Institute for Materials Science, 1-2-1 Sengen, Tsukuba, Ibaraki 305-0047, Japan*

[9]*National Synchrotron Radiation Research Center, Hsinchu 30076, Taiwan*

[10]*Department of Physics, National Tsing Hua University, Hsinchu 30013, Taiwan*

[11]*Synchrotron X-ray Station at SPring-8, National Institute for Materials Science, Kouto 1-1-1, Sayo-cho, Hyogo 679-5148, Japan*

[12]*Dresden Center for Computational Materials Science, DCMS, TU Dresden, D-01069 Dresden, Germany*

(Received 6 October 2016; published 28 December 2016)

The ferromagnetic semiconductor Ba_2NiOsO_6 ($T_{mag} \sim 100$ K) was synthesized at 6 GPa and 1500 °C. It crystallizes into a double perovskite structure [Fm-3m; $a = 8.0428(1)$ Å], where the Ni^{2+} and Os^{6+} ions are perfectly ordered at the perovskite B site. We show that the spin-orbit coupling of Os^{6+} plays an essential role in opening the charge gap. The magnetic state was investigated by density functional theory calculations and powder neutron diffraction. The latter revealed a collinear ferromagnetic order in a >21 kOe magnetic field at 5 K. The ferromagnetic gapped state is fundamentally different from that of known dilute magnetic semiconductors such as (Ga,Mn)As and (Cd,Mn)Te ($T_{mag} < 180$ K), the spin-gapless semiconductor Mn_2CoAl ($T_{mag} \sim 720$ K), and the ferromagnetic insulators EuO ($T_{mag} \sim 70$ K) and $Bi_3Cr_3O_{11}$ ($T_{mag} \sim 220$ K). It is also qualitatively different from known ferrimagnetic insulators and semiconductors, which are characterized by an antiparallel spin arrangement. Our finding of the ferromagnetic semiconductivity of Ba_2NiOsO_6 should increase interest in the platinum group oxides, because this alternative class of materials should be useful in the development of spintronic, quantum magnetic, and related devices.

DOI: 10.1103/PhysRevB.94.235158

I. INTRODUCTION

The study of dilute magnetic semiconductors has been motivated since the 1970s by the prospect that materials with tight coupling between magnetic and semiconducting properties may be useful in developing spintronic and related devices [1–3]. Early studies doped magnetic impurities into semiconducting hosts such as the III-V, II-VI, and IV semiconductors. Successful synthesis of a paramagnetic (II,Mn)-VI semiconductor was reported in 1978 followed by discovery of long-range ferromagnetic (FM) order at ∼10 K by Ohno *et al.* in 1992 [4]. The magnetic ordering temperature (T_{mag}) increased to 100 K by 1998 [3], but the T_{mag} of most dilute magnetic semiconductors to date remains at or below ∼180 K [5].

The variety of magnetic semiconductors has increased in concert with ongoing studies of dilute magnetic semiconductivity. For example, a "spin-gapless semiconductor" has been produced by synthesis of the Heusler alloy, Mn_2CoAl, which exhibits spin polarized transport at room temperature and holds promise for spintronic applications [6]. In 2007, a Co-doped TiO_2 film was claimed to show FM order at room temperature [7]. However, the essential mechanism of its ferromagnetism is still debated [8,9]. Attempts to apply the popular FM insulator EuO ($T_{mag} \sim 70$ K) [10] to technological use are in progress. La_2NiMnO_6 [11,12] and Bi_2NiMnO_6 [13–15] have been studied, because they have the potential to act as a FM insulator in practical applications. $Bi_3Cr_{2.91}O_{11}$ recently has been suggested to be a FM insulator with $T_{mag} \sim 220$ K [16]. In this study, we successfully synthesize a FM oxide, Ba_2NiOsO_6, in which the charge gap is produced by a mechanism fundamentally different from that of any proposed to date for known FM insulators and semiconductors such as above. The unconventional origin of this property suggests significant feasibility in designing a practical room-temperature FM insulator because a few 3d-5d double perovskite oxides (DPOs) related to Ba_2NiOsO_6 also exhibit magnetic order far above room temperature (Table S1 in the Supplemental Material [17]) [18] as well as related 4d and 5d oxides $SrTcO_3$ ($T_{mag} \sim 1000$ K) [19] and $NaOsO_3$ ($T_{mag} = 410$ K) [20], yet magnetic interactions are still poorly understood.

We report here the high-pressure, high-temperature synthesis of the cubic DPO, Ba_2NiOsO_6, and its characterization

*Hai.FENG_nims@hotmail.com

†ghimire.mpg@gmail.com

‡Present Address: Department of Crystalline Materials Science, Nagoya University, Furo-cho, Chikusa-ku, Nagoya, Aichi 464-8603, Japan.

by measurement of bulk magnetic properties and by powder neutron and x-ray diffraction. A hexagonal phase of Ba_2NiOsO_6 (P-3m1; $a = 5.73$ Å and $c = 14.07$ Å) was synthesized without high pressure in 1980, but its magnetic properties were not investigated [21]. Density functional theory (DFT) calculations show that spin-orbit coupling (SOC) plays an essential role in generating the charge gap. To our knowledge, cubic Ba_2NiOsO_6 differs qualitatively from most ferrimagnetic (FIM) semiconductors, in which spins are ordered in an antiparallel fashion. Our findings point to an alternative class of FM insulators driven by a platinum group element that may be useful in the synthesis of practical magnetic semiconductors.

II. EXPERIMENT

Materials synthesis. Polycrystalline Ba_2NiOsO_6 was synthesized by solid-state reaction at high pressure from powders of BaO_2 (99%, Kojundo Chemical Lab. Co., Ltd., Japan), NiO (99.99%, Kojundo Chemical Lab. Co., Ltd., Japan), Os (99.95%, Heraeus Materials Technology, Germany), and $KClO_4$ (>99.5%, Kishida Chemical Co., Ltd., Japan). The powders were thoroughly mixed in a stoichiometric ratio ($BaO_2/NiO/Os/KClO_4 = 2 : 1 : 1 : 0.25$) and sealed in a Pt capsule within an Ar-filled glove box. The sealed capsule was gradually and isotropically compressed in a belt-type press (Kobe Steel, Ltd., Japan) to a pressure of 6 GPa. It was then heated at 1500 °C for 1 h, while maintaining the capsule pressure. After heating, the sample was quenched to 100 °C or below within several seconds followed by release of the pressure over a few hours. The resulting pellet was polycrystalline, dense, and well sintered.

X-ray and neutron diffraction analysis. A piece of Ba_2NiOsO_6 pellet was finely ground and rinsed with water to remove residual KCl. The final fine black powder was investigated by synchrotron x-ray diffraction (SXRD) at the BL15XU beamline facility, SPring-8, Japan. SXRD data were collected at ambient temperature using a high-precision Debye-Scherrer type diffractometer [22] and the "MYTHEN" one-dimensional detector [23]. The radiation wavelength was 0.652 98 Å, which was confirmed by a CeO_2 reference. The SXRD pattern was analyzed by the Rietveld method using "RIETAN-VENUS" software [24,25] Neutron powder diffraction (ND) was performed on a 5-g sample of Ba_2NiOsO_6 powder using the HB-2A diffractometer at the High Flux Isotope Reactor at the Oak Ridge National Laboratory at temperatures down to 4 K. Two wavelengths were selected using a Ge monochromator. A wavelength of 1.54 Å was used to provide sufficient reflections for an accurate crystal structure determination. A 2.41 Å wavelength was used for the magnetic structure determination in both zero field and applied fields up to 45 kOe. The ND data were analyzed using the Rietveld refinement program FULLPROF [26]. The magnetic structural representation analysis was performed using SARAH [27].

Materials properties characterization. X-ray absorption spectroscopy (XAS) at the Ni-$L_{2,3}$ and Os-L_3 edges was conducted at the BL07C and BL08B beamlines using the total electron yield and transmission method, respectively, in the National Synchrotron Radiation Research Center (NSRRC) in Taiwan. The Ni-$L_{2,3}$ spectrum of NiO and the Os-L_3 spectrum of Sr_2FeOsO_6 [28,29] were measured simultaneously as references for Ni^{2+} and Os^{5+}, respectively.

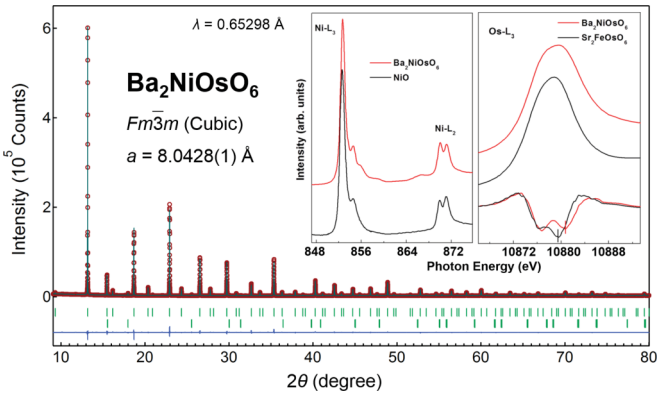

FIG. 1. The Rietveld refinement of the SXRD profile collected at room temperature for Ba_2NiOsO_6. The expected Bragg reflections are marked by ticks for Ba_2NiOsO_6 (top) and NiO (bottom). The estimated mass proportion was Ba_2NiOsO_6:NiO = 0.976 : 0.024. The insets depict the room temperature Ni-$L_{2,3}$ XAS spectra of Ba_2NiOsO_6 and NiO (Ni^{2+} reference) and the Os-L_3 XAS spectra of Ba_2NiOsO_6 and Sr_2FeOsO_6 (Os^{5+} reference) and their second derivative.

Other pieces of the Ba_2NiOsO_6 pellet were subjected to electrical resistivity (ρ) and specific heat (C_p) measurements. The ρ measurement was conducted at 100–300 K using a four-point method with a physical properties measurement system from Quantum Design, Inc. Electrical contacts were prepared longitudinally on a polycrystalline piece with Pt wires and silver paste. The dc gauge current was 0.1 mA. The temperature dependence of C_p was measured at 2–300 K by a thermal relaxation method. The contribution from residual KCl to the raw C_p data was subtracted using tabulated data [30] and the mole ratio (KCl:Ba_2NiOsO_6 = 0.25 : 1).

An amount of rinsed powder was subjected for magnetic studies; the magnetic susceptibility (χ) of Ba_2NiOsO_6 powder was measured with a magnetic property measurement system from Quantum Design, Inc. conducted in field-cooled (FC) and zero-field-cooled (ZFC) modes between 2 and 390 K in fixed magnetic fields of 0.1, 10, and 50 kOe. Isothermal magnetization was measured at 5, 50, and 200 K in magnetic fields between −50 kOe and +50 kOe with the same apparatus. Note that the mass fraction of NiO was 2.4% according to the SXRD analysis (see Fig. 1), indicating a small impurity level. Besides, NiO is an established antiferromagnetic (AFM) insulator; therefore, an AFM contribution at such a low concentration to the bulk properties was expected to be negligible. We hence did not correct raw magnetic data of the magnetic susceptibility and magnetization measurements.

Theoretical calculations. DFT calculations were carried out using the full-potential linearized augmented plane wave method as implemented in the WIEN2K code [31]. The atomic sphere radii (R_{MT}) were fixed at 2.5, 2.1, 2.0, and 1.63 Bohr radii for Ba, Ni, Os, and O, respectively. The linear tetrahedron method with 3000 (1000, 500) k points in the entire Brillouin

zone was employed for the reciprocal space integrations in the case of a cubic unit cell containing one chemical unit cell (and two for tetragonal and four for orthorhombic unit cells). The standard generalized gradient approximation (GGA) in the parametrization of Perdew, Burke, and Ernzerhof (PBE-96) [32] was used in the initial calculations. The GGA + U functional with double counting corrections according to Anisimov *et al.* [33] (a variant of the so-called fully localized limit with $J = 0$) was applied for the main investigations. Values of the screened Coulomb interaction $U = 5$ and 2 eV were used for the Ni and Os atoms, respectively. The calculations were tested by varying these values between 4 and 7 eV for Ni and 1 and 4 eV for Os, respectively. These ranges are comparable to values reported for 3*d* and 5*d* oxides ∼2−10 eV for 3*d* and ∼1−3 eV for 5*d*) [34–36]. SOC was considered via a second variational step using the scalar relativistic eigenfunctions as basis. All calculations were conducted using the experimental lattice parameters obtained at 4 K. Parts of the calculations were double checked with the full-potential local-orbital (FPLO) code [37]. Here, the linear tetrahedron method was employed with an $8 \times 8 \times 6k$ mesh. Results obtained from the WIEN2K code were found to agree well with those from the FPLO code.

III. RESULTS AND DISCUSSION

The crystal structure of Ba_2NiOsO_6 was refined by the Rietveld technique on an SXRD profile collected at room temperature. The SXRD pattern is shown in Fig. 1, and the refined crystallographic parameters are listed in Table I. The results indicate that Ba_2NiOsO_6 crystallizes in a fully ordered double perovskite structure, which is cubic with space group Fm-3m (similar to many other DPOs) [38,39]. The degree of order of the Ni and Os atoms was carefully investigated in the refinement procedure. First, the atoms were assumed to occupy the 4*a* and 4*b* crystallographic sites randomly and partially at equimolar ratio. Then, a fully ordered model, in which Ni remained solely at the 4*b* site and Os at the 4*a* site, was tested. The fully ordered model was found to provide the best refinement quality. We therefore conclude that Ba_2NiOsO_6 has fully ordered Ni and Os atoms, similar to Sr_2NiOsO_6 and Ca_2NiOsO_6 [40]. The order has been attributed to distinctive differences between the charge, size, and electronic configuration of the Ni and Os atoms [39,40].

The local coordination at the magnetic Ni and Os ions was investigated. The Os-O bond length [1.943(2) Å] was similar to values of 1.948 and 1.955 Å for the Os^{6+}-O bond in Ba_2CaOsO_6 [41] and Ba_2CuOsO_6 [42], respectively, rather than 1.963 Å for the Os^{5+}-O bond in Ba_2YOsO_6 [43]. This suggests that Os is nearly hexavalent. The bond valence sum (BVS) of Os was 5.72 [44], which also suggests hexavalency. The Ni-O bond length was 2.078(2) Å, which is comparable to 2.097 Å for the Ni^{2+}-O bond in Ba_2NiWO_6 [45] and distinctively different from 1.960 and 1.976 Å for the Ni^{3+}-O bond in $LaNiO_3$ [46] and $LiNiO_2$ [47], respectively. (We could not find any references for $Ba_2Ni^{3+}MO_6$ in accessible databases or the literature.) The BVS of Ni was 2.07, which indicates that Ni is nearly divalent. To ensure charge compensation in bulk, the valence distribution should be nominally +2 and +6 for Ni and Os, respectively. Therefore, the formal electronic configurations should be $3d^8$ ($t_{2g}^6\ e_g^2$; $S = 1$) for Ni, provided that the exchange splitting is smaller than the crystal field splitting (CFS), and $5d^2$ ($t_{2g}^2\ e_g^0$; $S = 1$) for Os. (Here and throughout the paper, we use the term CFS in the usual meaning that includes both electrostatic and hybridization effects.) The parameters $R_0(Ni^{2+}) = 1.675$ Å, $R_0(Os^{6+}) = 1.925$ Å, and $B = 0.37$ were used in the BVS calculations [44].

To further examine the valence states of Ni and Os in Ba_2NiOsO_6, we measured the Ni-$L_{2,3}$ and Os-L_3 XAS spectra together with those of reference materials (see the insets in Fig. 1). The identical energy positions and analogous multiplet spectral structures of the Ni-$L_{2,3}$ edges of Ba_2NiOsO_6 and NiO demonstrate the same Ni^{2+} valence state and NiO_6 local symmetry in both compounds. In contrast, a spectral shift at the Os-L_3 edge of approximately 1.0(1) eV to higher energy from Sr_2FeOsO_6 to Ba_2NiOsO_6 indicates an increased valency of 1 from Os^{5+} to Os^{6+} in the latter [48–51]. The energy shift, the CFS, and the relative t_{2g} and e_g related spectral weights can be clearly discerned in the second derivative spectra at the bottom of the right inset in Fig. 1. The e_g related peak is shifted by 1.3(1) eV to higher energy in Ba_2NiOsO_6 relative to Sr_2FeOsO_6, and the spectral weight of the t_{2g} related peak

TABLE I. Atomic positions and thermal parameters of Ba_2NiOsO_6. Note: Space group: Fm-3m; lattice parameter $a = 8.0428(1)$ Å, $Z = 4$; $d_{cal} = 7.9102\ g\,cm^{-3}$. R indices were $R_p = 2.82\%$ and $R_{wp} = 3.98\%$.

Atom	Site	Occupancy	x	y	z	B (Å^2)
Ba	8*c*	1	0.25	0.25	0.25	0.36(6)
Os	4*a*	1	0	0	0	0.11(4)
Ni	4*b*	1	0.5	0	0	0.19(2)
O	24*e*	1	0.2415(3)	0	0	0.40(2)

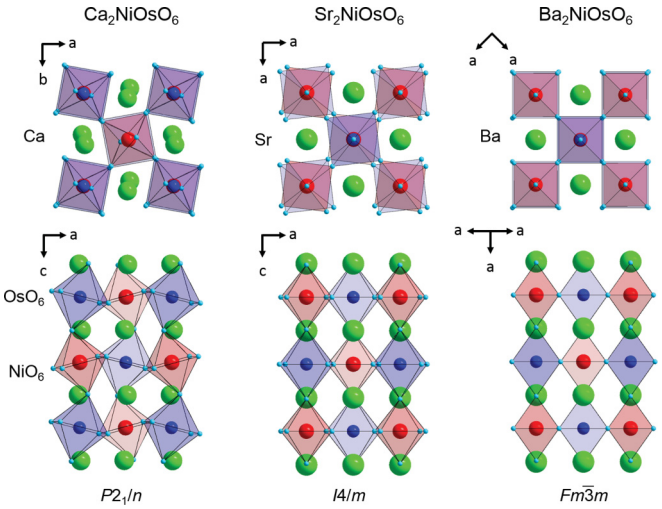

FIG. 2. Structural comparison of the series A_2NiOsO_6 (A = Ca, Sr, Ba). The crystal structure symmetry changes from monoclinic ($P2_1/n$) to cubic (Fm-3m) via a tetragonal ($I4/m$) symmetry. Green balls represent A atoms; reddish and bluish octahedra represent NiO_6 and OsO_6.

increases reflecting a smaller number of t_{2g} holes [48] on Os^{5+} (t_{2g}^3) compared to Os^{6+} (t_{2g}^2). The second derivative spectra show also a larger CFS for Os^{6+} in Ba_2NiOsO_6 compared with that of Os^{5+} in Sr_2FeOsO_6 as found in observations of Ir oxides [48].

We have compared the crystal structure of Ba_2NiOsO_6 with those of A_2NiOsO_6 (A = Ca, Sr) [40]. The crystal structure symmetry changes from monoclinic ($P2_1/n$; A = Ca) to cubic (Fm-$3m$; Ba) via a tetragonal ($I4/m$; Sr) symmetry, as shown in Fig. 2. An analogous symmetry change has been observed for A_2FeMoO_6 (A = Ca, Sr, Ba) [38], which suggests that the size of A plays a role in determining the lattice symmetry. The angle of the magnetic Os-O-Ni bond is altered from 151° (Ca_2NiOsO_6, monoclinic) [40] to 180° (Ba_2NiOsO_6, cubic) via 166°/180° (Sr_2NiOsO_6, tetragonal) [40]. The angle variation seems to have a large impact on the magnetic properties. For example, Ca_2NiOsO_6 is canted AFM below 175 K, whereas Sr_2NiOsO_6 is AFM below 50 K. When the size of A increases, the magnitude of the FM interaction increases as evidenced by the increase in Weiss temperature from 27 K in Sr_2NiOsO_6 (see Table S1 [17]) to 113(1) K in Ba_2NiOsO_6 [see the inset of Fig. 3(a)]. The Curie constant deduced from the 50 kOe FC curve for Ba_2NiOsO_6 is 1.48(2) emu mol^{-1} K^{-1}, which corresponds to an effective moment (μ_{eff}) of 3.46(2) μ_B per formula unit (f.u.). The Weiss temperature and the Curie constant deduced from the 0.1 kOe FC curve were 121(2) K and 1.28(2) emu mol^{-1} K^{-1} [μ_{eff} = 3.21(2) μ_B perf.u.], respectively, consistent with the absence of a marked change.

Although the FM interaction is large in Ba_2NiOsO_6, an AFM-like peak was observed in both the ZFC and FC curves at ~32 K (T_{mag}) (Fig. S1 [17]). However, no noticeable peak is present in the 50 kOe curves [Fig. 3(a)], which suggests a possible change of the magnetic order. To investigate the magnetism further, we conducted an isothermal magnetization measurement at a temperature below T_{mag}. The magnetization of Ba_2NiOsO_6 reaches approximately 2.3 μ_B f.u.$^{-1}$ at 50 kOe [at 5 K, Fig. 3(b)]. Intriguingly, the magnetic loop indicates a noticeable metamagnetic transition at approximately ±21 kOe for Ba_2NiOsO_6. For comparison, magnetic loops collected at 5 K for Sr_2NiOsO_6 and Ca_2NiOsO_6 are shown to emphasize the anomalous behavior of Ba_2NiOsO_6. A similar metamagnetic transition was observed for another DPO, R_2CoMnO_6 (R = rare-earth element). However, this was argued to be caused by the presence of significant antisite disorder [52–55]. Since such disorder is absent in Ba_2NiOsO_6, the origin of metamagnetism of Ba_2NiOsO_6 should be different.

We also conducted specific heat measurements near T_{mag} with and without application of a magnetic field (Fig. S2 [17]). The zero-magnetic field curve shows a broad cusp at ~32 K, whereas the cusplike top shifts slightly toward lower temperature in an applied field of 10 kOe. In magnetic fields of 30 and 50 kOe, the cusp disappears completely. The disappearance is likely connected to the absence of an AFM-like peak on the χ-T curves at 50 kOe.

The temperature dependence of the electrical resistivity of polycrystalline Ba_2NiOsO_6 is shown in Fig. 4 . At room temperature the value is ~120 Ω cm, which is more than three orders of magnitude greater than the expected value

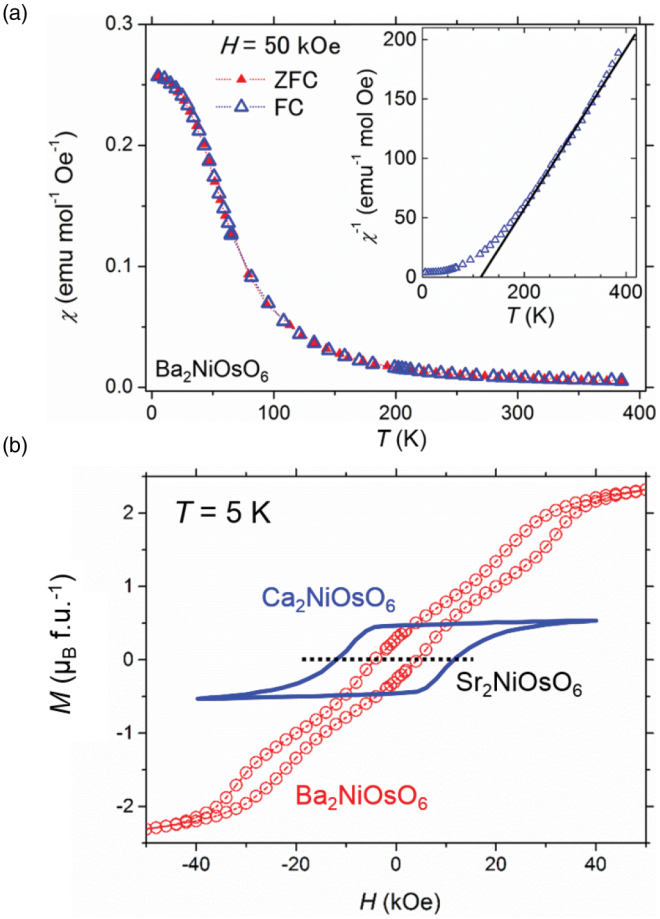

FIG. 3. (a) Temperature dependence of the magnetic susceptibility of Ba_2NiOsO_6 measured at 50 kOe. The inset shows the inverse magnetic susceptibility. The solid line is the Curie-Weiss fit to the curve. (b) Isothermal magnetization loop of Ba_2NiOsO_6 at 5 K in comparison with the loops for Ca_2NiOsO_6 (taken from Ref. [39]) and Sr_2NiOsO_6 (estimated from the magnetic susceptibility data in Ref. [39]).

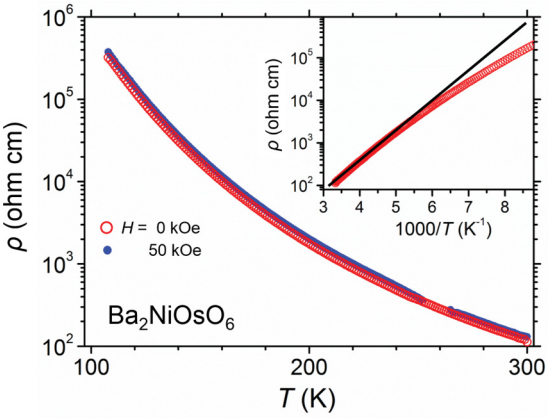

FIG. 4. The temperature dependence of ρ for polycrystalline Ba_2NiOsO_6. The inset shows the Arrhenius plot of the data and the fitting line, which yield an activation energy of 0.31 eV. Data measured in a magnetic field of 50 kOe also are presented.

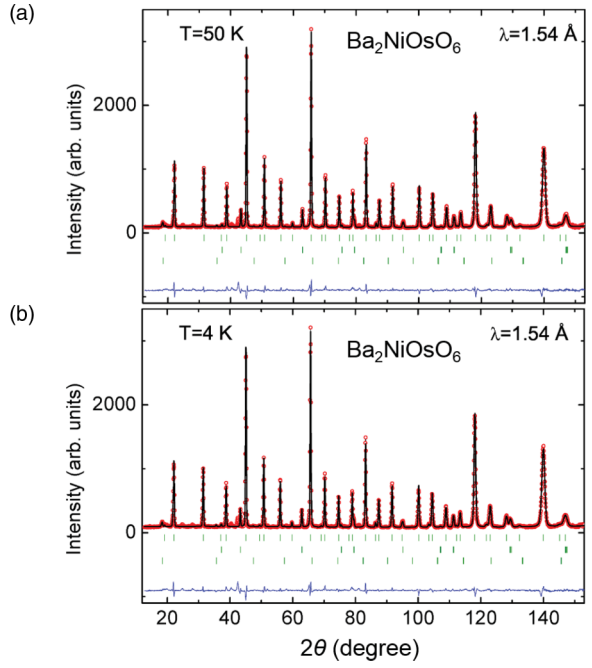

FIG. 5. Rietveld refinement of the ND profiles (λ = 1.54 Å) of Ba_2NiOsO_6 collected at temperatures of (a) 50 K and (b) 4 K. The expected Bragg reflections are marked by ticks for Ba_2NiOsO_6 (top), NiO (middle), and the magnetic lattice of NiO (bottom).

for a metallic polycrystalline oxide. Electrical resistivity increased upon cooling and exceeded the instrumental limit at temperatures below 105 K indicating a semiconductorlike behavior. To estimate the activation energy of conduction, data points were plotted on a logarithmic scale as a function of inverse temperature and fit to the Arrhenius equation. The fit provided an activation energy of 0.31 eV (see the inset of Fig. 4). In a field of 50 kOe, the electrical resistivity remained high and exceeded the instrumental limit at low temperatures as in zero field (see the plot of solid circles).

The magnetic order of Ba_2NiOsO_6 was investigated by ND at low temperatures. Figures 5(a) and 5(b) show the ND patterns (λ = 1.54 Å) collected at 50 and 4 K, respectively. The nuclear lattice was well refined by the room-temperature lattice model both above and below the AFM-like peak temperature (∼32 K), which indicates the absence of a lattice symmetry change down to 5 K regardless of the presence of the magnetic transition. Although the electronic configuration of Os^{6+} ($5d\ t_{2g}^2$) implies a possible orbital order below T_{mag} [56,57]; any indication of reduced lattice symmetries lower than cubic was undetected within the instrument resolution. For example, a refinement attempt with a tetragonal space group of $I4/m$ did not converge to stable lattice parameters. A robust cubic symmetry lattice, which argues against orbital ordering, was found in a similar Os^{6+} compound, Ba_2CaOsO_6 [58]. The low-temperature crystallographic parameters are summarized in Table S2 [17].

After changing λ to 2.41 Å, we conducted ND measurements to investigate the magnetic order. The difference between the profiles at 5 and 75 K clearly revealed the presence of modulated AFM order as shown in Fig. S4 (detailed analysis is provided in the Supplemental Material [17]). The modulated AFM order transformed to a collinear FM order in a magnetic field above 21 kOe at 5 K. For example, the difference between the zero-field and non-zero-field ND profiles clearly revealed the presence of FM order [Fig. 6(a)], which gradually developed with increasing magnetic field [Fig. 6(b)]. Figure 6(c) shows the applied magnetic field dependence of the magnetic peak intensity at $2\theta = 30^\circ$, which indicates that the critical field (H_c) is 21 kOe at 5 K. The magnetic field observations throughout the ND measurements accord well with the metamagnetic transition found in the isothermal magnetization measurements. The FM order also was refined by analysis of the ND profile collected at 45 kOe. All Ni and Os magnetic moments lie along the [100] or equivalent [010] or [001] direction [Fig. 6(d)] indicating the common plane of the modulated AFM and FM orders.

The magnetic moments in the FM state at 5 K were estimated to be 2.13(8) and 0.97(5) μ_B per Ni and Os, respectively. Although the Ni moment is comparable to the spin only moment estimated from a simplified model, the Os moment is significantly smaller. This is most likely due to the impact of the SOC of Os, as suggested in Ref. [59], and to the extended orbitals of the $5d$ atom leading to increased hybridization, as suggested in Ref. [60]. The magnetization of Ba_2NiOsO_6 at 5 K and 50 kOe is approximately 2.3 μ_B f.u.$^{-1}$ [Fig. 3(b)], although the ND analysis yields approximately 3 μ_B f.u.$^{-1}$ in total. This indicates incomplete saturation in a 50 kOe field, which is evident from the relatively large gradient, dM/dH, at this strength [see Fig. 3(b)]. Further high-field-magnetization studies may confirm the ND result.

We have analyzed the electronic and magnetic states of Ba_2NiOsO_6 by DFT. We calculated the total energies of supercells with magnetic alignments corresponding to one FM, two AFM, and three FIM orderings (see Fig. 7). Using up and down spins to indicate the magnetic moment on the Ni1, Ni2, Os1, and Os2 atoms, the orderings investigated are FM1-↑↑↑↑, AF1-↑↓↑↓, AF2-↑↓↓↑, FI1-↑↑↓↓, FI2-↑↓↑↑, and FI3-↑↑↑↓, respectively. These arrangements are considered in tetragonal supercells (space group 123, $P4/mmm$) containing two chemical unit cells. We double checked the calculations using orthorhombic supercells (space group 47, $Pmmm$) with four chemical unit cells and pseudocubic lattice parameters $a = b = c$. The two settings produced nearly identical results (with differences below 4 meV f.u.$^{-1}$) for calculations conducted without SOC. With SOC, the total energies obtained with the tetragonal setting did not fulfill the expected symmetry relations. Thus, we report only results obtained with the orthorhombic setting. The latter was double checked by performing GGA + U + SOC calculations in a cubic cell with one chemical unit for the FM1 case. The magnetic anisotropy energies were 18 meV f.u.$^{-1}$ (orthorhombic setting; see Table II) and 13 meV f.u.$^{-1}$ (cubic setting). From this comparison and the small differences between the orthorhombic and tetragonal settings, we assume that the other energy differences in Table II have a similar precision of ca. 5 meV f.u.$^{-1}$.

By comparing the total energies of the different magnetic arrangements, we find that the FM1 order has the lowest total energy regardless of the calculation scheme (Table II). The energy difference to the next lowest order (AF2) is very small, ∼16 meV per f.u. in GGA + U + SOC. The difference

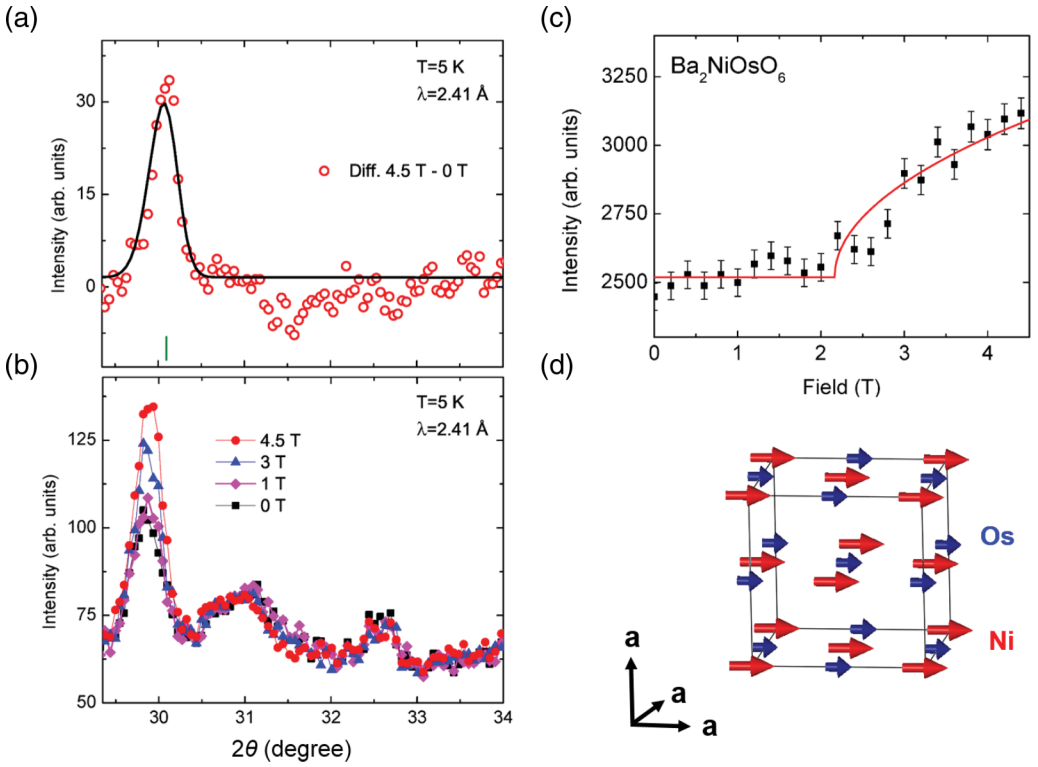

FIG. 6. (a) Difference between the zero-field profile and the profile collected in a magnetic field of 45 kOe at 5 K. (b) Evolution of a magnetic peak with increasing magnetic field at 5 K. (c) Magnetic field dependence of the intensity of the magnetic peak at $2\theta = 30^\circ$ ($\lambda = 2.41$ Å) at a fixed temperature of 5 K. The solid line and curve are a guide for the eyes. (d) Magnetic order model of the FM state of Ba_2NiOsO_6 depicted from the analysis of the ND profiles. The magnetic easy axis lies in the cubic [100], [010], or [001] direction.

is almost comparable to the precision of the method, which implies a competition between the FM1 and AF2 orders. Other possible magnetic orders (not shown here) were found at much higher energies and were excluded from further investigation.

The FM1 alignment is identical to the experimental FM state in an external magnetic field [Fig. 6(d)]. Figure 8 shows the DOS of FM1 for cases (a) without and (b) with SOC. The band structures in Figs. 9(a) and 9(b) show a metallic state for GGA + U and a gapped state for GGA + U + SOC. For a more detailed view, we considered the partial DOS (Fig. S7 [17]). The Ni 3d band is fully occupied in one spin channel and partially occupied (nominally $t_{2g}^3\ e_g^0$) in the other, both with and without SOC. Due to the combined effect of CFS and $U = 5$ eV, the unoccupied Ni e_g states lie about 2 eV above E_F. The O 2p orbitals hybridize strongly with the Ni 3d orbitals below -1.5 eV (the valence region) and with the Os 5d orbitals.

The most interesting band located at the Fermi level is composed mainly of Os 5d states (Fig. S7 [17]). We performed a decomposition into ml-states (Fig. S8 [17]), which confirms the expected t_{2g} character of the band. Without SOC [Fig. 9(a)], the Os t_{2g} states form two band complexes, each containing

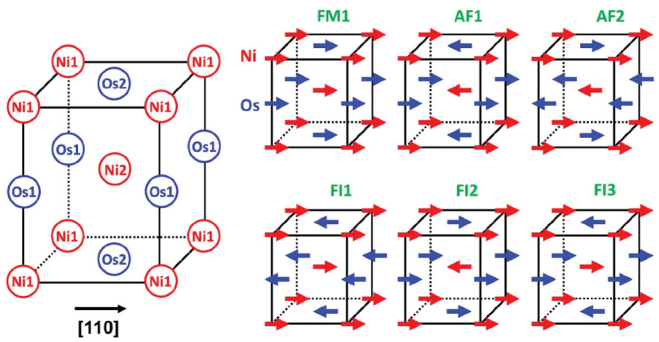

FIG. 7. Left: Sketch of the tetragonal supercell (space group 123, $P4/mmm$) used for DFT calculations of possible magnetic arrangements. The cubic [110] direction is indicated. Right: Schematic of the magnetic arrangements. Red and blue arrows indicate magnetic moments on the Ni/Os atoms. The magnetic easy axis was found to lie along the cubic [110] direction for FM1 and AF2 by GGA + U + SOC.

TABLE II. Relative total energies (meV f.u.$^{-1}$) calculated within GGA, GGA + U, and GGA + U + SOC schemes for Ba_2NiOsO_6. For the latter scheme, the orientations of the magnetic moments are given with respect to the cubic axes. Results for the [110] orientation were obtained only for the three spin arrangements with the lowest energies in GGA or GGA + U.

	FM1	AF1	AF2	FI1	FI2	FI3
GGA	0	85	40	115	61	58
GGA + U	0	73	45	82	58	40
GGA + U + SOC [001]	18	68	41	91	55	53
GGA + U + SOC [100]	18	48	25	91	37	52
GGA + U + SOC [110]	0		16			28

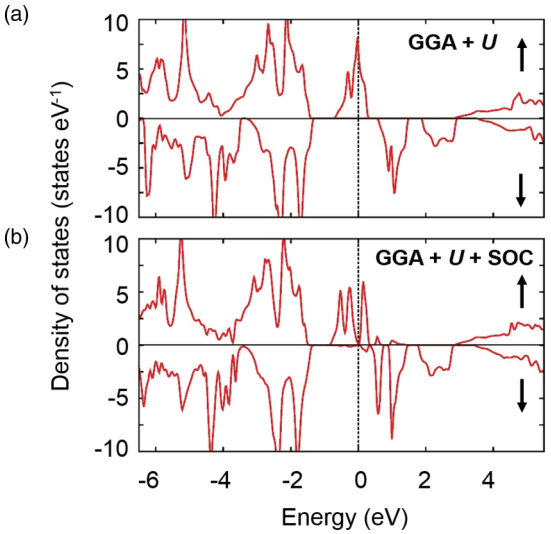

FIG. 8. The total DOS (per f.u.) for spin-up (↑) and spin-down (↓) channels of the FM1 state of Ba_2NiOsO_6 obtained in the (a) GGA + U and (b) GGA + U + SOC schemes. The vertical dotted line indicates $E_F = 0$.

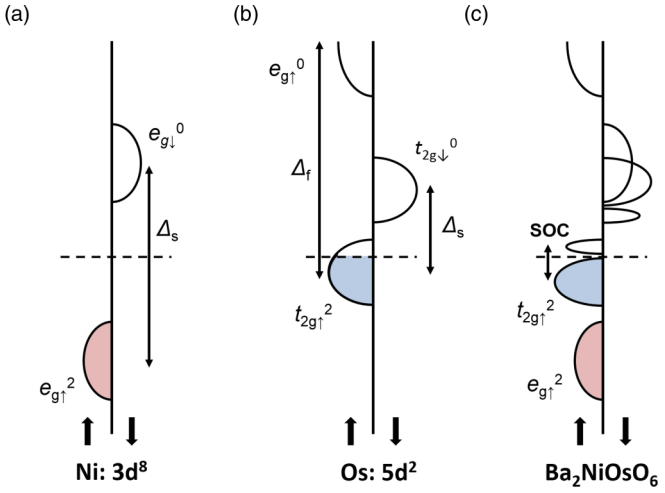

FIG. 10. A schematic view of the d band DOS structure of the FM1 state of Ba_2NiOsO_6. The partial DOS for (a) Ni 3d and (b) Os 5d bands and (c) the total DOS. The symbols Δ_s and Δ_f represent the spin exchange splitting and crystal field splitting (including correlation effects), respectively.

three individual bands: a spin-up complex around the Fermi level and a spin-down complex around 1 eV. The former is partially occupied with two electrons per Os. It cannot be split without breaking the nonrelativistic cubic symmetry, such that application of U does not open a gap. With SOC [Fig. 9(b)], the t_{2g} states are split into two Γ_8 states and one Γ_7 state. However, SOC alone is not sufficient to open a gap, because the band dispersion is greater than the spin-orbit splitting, which leads to an (indirect) overlap of the band states. Although we could not directly measure the strength of the SOC from the calculation, a comparison between the degree of splitting of the t_{2g} band within the GGA and GGA + SOC schemes roughly estimates the spin-orbit splitting to be ∼0.17 eV. Due to symmetry reduction upon inclusion of SOC, application of Coulomb corrections may increase the splitting between occupied and unoccupied bands, which will open the gap at a certain value of U. A schematic illustration of the mechanism is depicted in Fig. 10. For the sake of clarity, details of the DOS are ignored or changed, and the oxygen DOS is omitted.

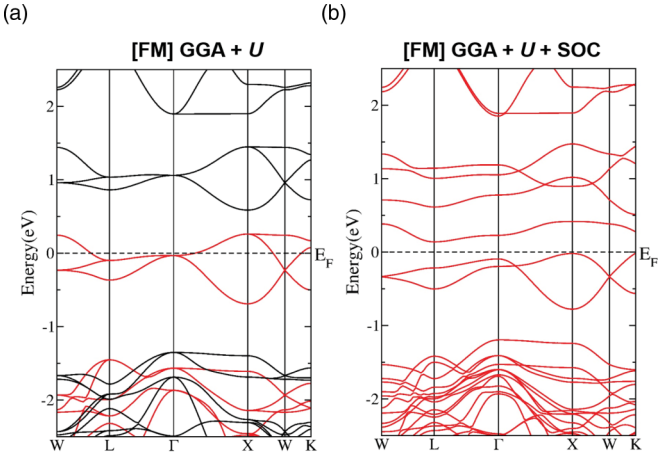

FIG. 9. Band structures of the FM1 state of Ba_2NiOsO_6 within (a) GGA + U (red: spin up; black: spin down) and (b) GGA + U + SOC. Dashed horizontal lines at zero correspond to E_F.

IV. CONCLUSION

Cubic Ba_2NiOsO_6 was synthesized by solid-state reaction at 6 GPa and 1500 °C. SXRD and ND revealed cubic lattice symmetry (Fm-$3m$) with lattice parameter $a = 8.0428(1)$ Å at room temperature [8.0298(1) Å at 4 K]. XAS of the Ni and Os core levels indicated that the formal charges on Ni and Os are essentially +2 and +6, respectively. Thus, the formal electronic configurations should be $3d^8$ (t_{2g}^6 e_g^2; $S = 1$) for Ni and $5d^2$ (t_{2g}^2 e_g^0; $S = 1$) for Os. The combined evaluation of theoretical and experimental results establish Ba_2NiOsO_6 as a FM insulator with T_{mag} of ∼100 K. SOC plays an essential role in opening the charge gap. A metamagnetic transition was found at 5 K, where a modulated AFM state transforms to the FM state at a moderate magnetic field (H_c ∼ 21 kOe at 5 K) without altering the semiconducting property. DFT calculations suggest that FM and helical AFM orders have comparable total energies and are responsible for the metamagnetic transition. We conclude that both Coulomb and relativistic effects must be considered equally in Ba_2NiOsO_6. The situation is similar to the cases of the platinum group oxide Sr_2IrO_4 [36,61,62] and α-$RuCl_3$ [63], although these are essentially AFM materials.

Recently, a similar material, Ba_2NaOsO_6, having $5d^1$ (t_{2g}^1 t_g^0) configuration of Os, has theoretically been studied, suggesting that it is an uncommon FM insulator [64]. Although the Weiss temperature of Ba_2NaOsO_6 is weakly negative (−10 K), it might be the first material being clarified as a FM Dirac-Mott insulator ($T_{mag} = 6.8$ K). The present compound is likely the second case; however, the FM properties are dramatically improved as evidenced by such things as the substantially positive Weiss temperature (+113 K) and increased T_{mag} near

100 K. Thus, the cubic double perovskite reported here could be useful to deepen understanding of the nature of the FM Dirac-Mott insulator.

Cubic Ba_2NiOsO_6 should increase general interest in platinum group oxides. Platinum group metals and their complexes have been used in many practical applications, because of their excellent catalytic activities [65]. However, electrical properties and other practical features are not well known apart from high electrical conductivity and robust corrosion resistance. Recent studies of Ir and Os oxides have shown that the significant SOC and extended 5*d* orbitals in the oxide produce outstanding electric and magnetic properties as found in Slater insulators [20,66], Dirac-Mott insulators [36,61], and ferroelectric metals [67]. The largest reported spin-phonon-electron coupling was recently discovered in an osmium oxide, which further illustrates this potential of high-valent platinum group oxides [68]. Growing interest in unique physical properties, as exemplified by the FM semiconductivity of cubic Ba_2NiOsO_6, should motivate further study of platinum group oxides. Our report of cubic Ba_2NiOsO_6 heralds an alternative class of FM insulator oxides, which may be useful in developing a practical magnetic semiconductor that can be employed in spintronic and quantum magnetic devices.

ACKNOWLEDGMENTS

The authors would like to thank the staff of BL15XU, NIMS, and SPring-8 for their help at the beamline. The SXRD measurements were performed under the approval of the NIMS Beamline Station (Proposals No. 2014A4504, NO. 2014B4501, No. 2015A4502, and No. 2016B4504). The XAS measurements were supported by Chin-Wen Pao. M.P.G thanks the Alexander von Humboldt Foundation for financial support through the Georg Forster Research Fellowship Program. M.P.G. thanks K. Koepernik and R. Laskowski for helpful discussion, and M.R. thanks M. Knupfer, U. Rößler, and H. Rosner for helpful discussion. M.P.G. and M.R. thank U. Nitzsche for technical assistance. This research was supported in part by the World Premier International Research Center of the Ministry of Education, Culture, Sports, Science and Technology (MEXT) of Japan and the Japan Society for the Promotion of Science (JSPS) through a Grant-in-Aid for Scientific Research (Grants No. 25289233, No. 15K14133, and No. 16H04501). The research conducted at ORNL's High Flux Isotope Reactor was sponsored by the Scientific User Facilities Division, Office of Basic Energy Sciences, US Department of Energy.

[1] T. Dietl, Nat. Mater. **9**, 965 (2010).
[2] A. H. MacDonald, P. Schiffer, and N. Samarth, Nat. Mater. **4**, 195 (2005).
[3] H. Ohno, Science **281**, 951 (1998).
[4] H. Ohno, H. Munekata, T. Penney, S. von Molnár, and L. L. Chang, Phys. Rev. Lett. **68**, 2664 (1992).
[5] M. Wang, R. P. Campion, A. W. Rushforth, K. W. Edmonds, C. T. Foxon, and B. L. Gallagher, Appl. Phys. Lett. **93**, 132103 (2008).
[6] S. Ouardi, G. H. Fecher, C. Felser, and J. Kübler, Phys. Rev. Lett. **110**, 100401 (2013).
[7] Y. Matsumoto, M. Murakami, T. Shono, T. Hasegawa, T. Fukumura, M. Kawasaki, P. Ahmet, T. Chikyow, S.-y. Koshihara, and H. Koinuma, Science **291**, 854 (2001).
[8] M. Parras, Á. Varela, R. Cortés-Gil, K. Boulahya, A. Hernando, and J. M. González- Calbet, J. Phys. Chem. Lett. **4**, 2171 (2013).
[9] S. R. Shinde, S. B. Ogale, J. S. Higgins, H. Zheng, A. J. Millis, V. N. Kulkarni, R. Ramesh, R. L. Greene, and T. Venkatesan, Phys. Rev. Lett. **92**, 166601 (2004).
[10] N. Tsuda, K. Nasu, A. Fujimori, and K. Siratori, *Electronic Conduction in Oxides* (Springer, Berlin, 2013).
[11] R. I. Dass and J. B. Goodenough, Phys. Rev. B **67**, 014401 (2003).
[12] R. I. Dass, J. Q. Yan and J. B. Goodenough, Phys. Rev. B **68**, 064415 (2003).
[13] E. Langenberg, I. Fina, J. Ventura, B. Noheda, M. Varela, and J. Fontcuberta, Phys. Rev. B **86**, 085108 (2012).
[14] Y. Du, Z. X. Cheng, X. L. Wang, P. Liu, and S. X. Dou, J. Appl. Phys. **109**, 07B507 (2011).
[15] M. Azuma, K. Takata, T. Saito, S. Ishiwata, Y. Shimakawa, and M. Takano, J. Am. Chem. Soc. **127**, 8889 (2005).
[16] W. Yi, Y. Matsushita, A. Sato, K. Kosuda, M. Yoshitake, and A. A. Belik, Inorg. Chem. **53**, 8362 (2014).
[17] See Supplemental Material at http://link.aps.org/supplemental/10.1103/PhysRevB.94.235158 for list of double perovskite oxides, A_2MOsO_6, in which A = Ca, Sr, Ba, and M = a 3d-transition metal.
[18] D. Serrate, J. M. De Teresa, and M. R. Ibarra, J. Phys.: Condens. Matter. **19**, 023201 (2007).
[19] E. E. Rodriguez, F. Poineau, A. Llobet, B. J. Kennedy, M. Avdeev, G. J. Thorogood, M. L. Carter, R. Seshadri, D. J. Singh, and A. K. Cheetham, Phys. Rev. Lett. **106**, 067201 (2011).
[20] Y. G. Shi, Y. F. Guo, S. Yu, M. Arai, A. A. Belik, A. Sato, K. Yamaura, E. Takayama-Muromachi, H. F. Tian, H. X. Yang, J. Q. Li, T. Varga, J. F. Mitchell, and S. Okamoto, Phys. Rev. B **80**, 161104 (2009).
[21] U. Treiber and S. Kemmler-Sack, Z. Anorg. Allg. Chem. **470**, 95 (1980).
[22] M. Tanaka, Y. Katsuya, and A. Yamamoto, Rev. Sci. Instrum. **79**, 075106 (2008).
[23] M. Tanaka, Y. Katsuya, Y. Matsushita, and O. Sakata, J. Ceram. Soc. Jpn. **121**, 287 (2013).
[24] K. Momma and F. Izumi, J. Appl. Crystallogr. **41**, 653 (2008).
[25] F. Izumi and K. Momma, Solid State Phenom. **130**, 15 (2007).
[26] J. Rodríguez-Carvajal, Physica B **192**, 55 (1993).
[27] A. S. Wills, Physica B **276-278**, 680 (2000).
[28] A. K. Paul, M. Reehuis, V. Ksenofontov, B. H. Yan, A. Hoser, D. M. Tobbens, P. M. Abdala, P. Adler, M. Jansen, and C. Felser, Phys. Rev. Lett. **111**, 167205 (2013).
[29] A. K. Paul, M. Jansen, B. H. Yan, C. Felser, M. Reehuis, and P. M. Abdala, Inorg. Chem. **52**, 6713 (2013).
[30] Y. S. Touloukian and E. H. Buyco, *Specific Heat Nonmetallic Solids* (IFI/Plenum, New York, 1970).
[31] P. Blaha, K. Schwarz, G. K. H. Madsen, D. Kvasnicka, and J. Luitz, *WIEN2k, version 14.2, An Augmented Plane Wave+Local*

Orbitals Program for Calculating Crystal Properties (Technische Universitat Wien, Austria, 2001).
[32] J. P. Perdew, K. Burke, and M. Ernzerhof, Phys. Rev. Lett. **77**, 3865 (1996).
[33] V. I. Anisimov, I. V. Solovyev, M. A. Korotin, M. T. Czyzyk, and G. A. Sawatzky, Phys. Rev. B **48**, 16929 (1993).
[34] Y. Yuan, H. L. Feng, M. P. Ghimire, Y. Matsushita, Y. Tsujimoto, J. He, M. Tanaka, Y. Katsuya, and K. Yamaura, Inorg. Chem. **54**, 3422 (2015).
[35] H. B. Wang, S. S. Zhu, X. D. Ou, and H. Wu, Phys. Rev. B **90**, 054406 (2014).
[36] B. J. Kim, H. Jin, S. J. Moon, J. Y. Kim, B. G. Park, C. S. Leem, J. Yu, T. W. Noh, C. Kim, S. J. Oh, J. H. Park, V. Durairaj, G. Cao, and E. Rotenberg, Phys. Rev. Lett. **101**, 076402 (2008).
[37] K. Koepernik and H. Eschrig, Phys. Rev. B **59**, 1743 (1999).
[38] R. P. Borges, R. M. Thomas, C. Cullinan, J. M. D. Coey, R. Suryanarayanan, L. Ben-Dor, L. Pinsard-Gaudart, and A. Revcolevschi, J. Phys.: Condens. Matter. **11**, L445 (1999).
[39] M. T. Anderson, K. B. Greenwood, G. A. Taylor, and K. R. Poeppelmeier, Prog. Solid State Chem. **22**, 197 (1993).
[40] R. Macquart, S. J. Kim, W. R. Gemmill, J. K. Stalick, Y. Lee, T. Vogt, and H. C. zur Loye, Inorg. Chem. **44**, 9676 (2005).
[41] K. Yamamura, M. Wakeshima, and Y. Hinatsu, J. Solid State Chem. **179**, 605 (2006).
[42] H. L. Feng, M. Arai, Y. Matsushita, Y. Tsujimoto, Y. H. Yuan, C. I. Sathish, J. F. He, M. Tanaka, and K. Yamaura, J. Solid State Chem. **217**, 9 (2014).
[43] E. Kermarrec, C. A. Marjerrison, C. M. Thompson, D. D. Maharaj, K. Levin, S. Kroeker, G. E. Granroth, R. Flacau, Z. Yamani, J. E. Greedan, and B. D. Gaulin, Phys. Rev. B **91**, 075133 (2015).
[44] I. D. Brown, Chem. Rev. **109**, 6858 (2009).
[45] D. E. Cox, G. Shirane, and B. C. Frazer, J. Appl. Phys. **38**, 1459 (1967).
[46] H. Falcón, A. E. Goeta, G. Punte, and R. E. Carbonio, J. Solid State Chem. **133**, 379 (1997).
[47] A. Hirano, R. Kanno, Y. Kawamoto, Y. Takeda, K. Yamaura, M. Takano, K. Ohyama, M. Ohashi, and Y. Yamaguchi, Solid State Ionics **78**, 123 (1995).
[48] L. S. I. Veiga, G. Fabbris, M. van Veenendaal, N. M. Souza-Neto, H. L. Feng, K. Yamaura, and D. Haskel, Phys. Rev. B **91**, 235135 (2015).
[49] J.-M. Chen, Y.-Y. Chin, M. Valldor, Z. Hu, J.-M. Lee, S.-C. Haw, N. Hiraoka, H. Ishii, C.-W. Pao, K.-D. Tsuei, J.-F. Lee, H.-J. Lin, L.-Y. Jang, A. Tanaka, C.-T. Chen, and L. H. Tjeng, J. Am. Chem. Soc. **136**, 1514 (2014).
[50] T. Burnus, Z. Hu, H. Wu, J. C. Cezar, S. Niitaka, H. Takagi, C. F. Chang, N. B. Brookes, H. J. Lin, L. Y. Jang, A. Tanaka, K. S. Liang, C. T. Chen, and L. H. Tjeng, Phys. Rev. B **77**, 205111 (2008).
[51] Z. Hu, M. S. Golden, S. G. Ebbinghaus, M. Knupfer, J. Fink, F. M. F. de Groot, and G. Kaindl, Chem. Phys. **282**, 451 (2002).
[52] M. K. Kim, J. Y. Moon, H. Y. Choi, S. H. Oh, N. Lee, and Y. J. Choi, J. Phys.: Condens. Matter. **27**, 426002 (2015).
[53] J. Blasco, L. Garcia-Munoz, J. Garcia, J. Stankiewicz, G. Subias, C. Ritter, and J. A. Rodriguez-Velamaz, Appl. Phys. Lett. **107**, 012902 (2015).
[54] L. Y. Wang, W. P. Zhou, D. H. Wang, Q. Q. Cao, Q. Y. Xu, and Y. W. Du, J. Appl. Phys. **117**, 17D914 (2015).
[55] H. S. Nair, T. Chatterji, and A. M. Strydom, Appl. Phys. Lett. **106**, 022407 (2015).
[56] M. A. Laguna-Marco, P. Kayser, J. A. Alonso, M. J. Martínez-Lope, M. van Veenendaal, Y. Choi, and D. Haskel, Phys. Rev. B **91**, 214433 (2015).
[57] S. I. Csiszar, M. W. Haverkort, Z. Hu, A. Tanaka, H. H. Hsieh, H. J. Lin, C. T. Chen, T. Hibma, and L. H. Tjeng, Phys. Rev. Lett. **95**, 187205 (2005).
[58] C. M. Thompson, J. P. Carlo, R. Flacau, T. Aharen, I. A. Leahy, J. R. Pollichemi, T. J. S. Munsie, T. Medina, G. M. Luke, J. Munevar, S. Cheung, T. Goko, Y. J. Uemura, and J. E. Greedan, J. Phys.: Condens. Matter. **26**, 306003 (2014).
[59] H. Matsuura and K. Miyake, J. Phys. Soc. Jpn. **82**, 073703 (2013).
[60] A. E. Taylor, R. Morrow, D. J. Singh, S. Calder, M. D. Lumsden, P. M. Woodward, and A. D. Christianson, Phys. Rev. B **91**, 100406 (2015).
[61] B. J. Kim, H. Ohsumi, T. Komesu, S. Sakai, T. Morita, H. Takagi, and T. Arima, Science **323**, 1329 (2009).
[62] G. Jackeli and G. Khaliullin, Phys. Rev. Lett. **102**, 017205 (2009).
[63] K. W. Plumb, J. P. Clancy, L. J. Sandilands, V. V. Shankar, Y. F. Hu, K. S. Burch, H. Y. Kee, and Y. J. Kim, Phys. Rev. B **90**, 041112 (2014).
[64] S. Gangopadhyay and W. E. Pickett, Phys. Rev. B **91**, 045133 (2015).
[65] H. Renner, G. Schlamp, I. Kleinwächter, E. Drost, H. M. Lüschow, P. Tews, P. Panster, M. Diehl, J. Lang, T. Kreuzer, A. Knödler, K. A. Starz, K. Dermann, J. Rothaut, R. Drieselmann, C. Peter, and R. Schiele, in *Ullmann's Encyclopedia of Industrial Chemistry*, edited by Barbara Elvers (Wiley-VCH Verlag GmbH & Co. KGaA, Berlin, 2000).
[66] S. Calder, V. O. Garlea, D. F. McMorrow, M. D. Lumsden, M. B. Stone, J. C. Lang, J. W. Kim, J. A. Schlueter, Y. G. Shi, K. Yamaura, Y. S. Sun, Y. Tsujimoto, and A. D. Christianson, Phys. Rev. Lett. **108**, 257209 (2012).
[67] Y. G. Shi, Y. F. Guo, X. Wang, A. J. Princep, D. Khalyavin, P. Manuel, Y. Michiue, A. Sato, K. Tsuda, S. Yu, M. Arai, Y. Shirako, M. Akaogi, N. L. Wang, K. Yamaura, and A. T. Boothroyd, Nat. Mater. **12**, 1024 (2013).
[68] S. Calder, J. H. Lee, M. B. Stone, M. D. Lumsden, J. C. Lang, M. Feygenson, Z. Zhao, J. Q. Yan, Y. G. Shi, Y. S. Sun, Y. Tsujimoto, K. Yamaura, and A. D. Christianson, Nat. Commun. **6**, 8916 (2015).